Journal of Molecular Structure 1245 (2021) 131013

Contents lists available at ScienceDirect

Journal of Molecular Structure

journal homepage: www.elsevier.com/locate/molstr

Synthesis, antifungal studies, molecular docking, ADME and DNA interaction studies of 4-hydroxyphenyl benzothiazole linked 1,2,3-triazoles

Nidhi Nehra [a], Ram Kumar Tittal [a,*], D. Ghule Vikas [a], Naveen [a], Kashmiri Lal [b]

[a] Department of Chemistry, National Institute of Technology Kurukshetra, Haryana,136119, India
[b] Department of Chemistry, Guru Jambheshwar University of Science & Technology, Hisar,125001, Haryana, India

ARTICLE INFO

Article history:
Received 17 May 2021
Revised 22 June 2021
Accepted 29 June 2021
Available online 5 July 2021

Keywords:
4-Hydroxyphenyl benzothiazole linked 1,2,3-triazole
Antifungal activity
14α- Sterol demethylase enzyme
DNA binding
Molecular docking

ABSTRACT

In search of new bioactive 1,2,3-triazole hybrids, some 4-hydroxyphenyl benzothiazole (4-HBT) linked 1,2,3-triazole with varying lengths of alkyl spacers were synthesized from bromo alkoxy derivatives of 4-HBT. All the synthesized hybrids were satisfactorily characterized, and were evaluated for *in-vitro* antifungal activity against *C. tropicalis* and *A. terreus* fungal strains wherein compound **4 h** showed better activity for both fungal strains compared to the reference drug Fluconazole. Molecular docking with the active site of 14α-sterol demethylase enzyme (PDBID: 1EA1) showed that all compounds exhibited strong H-bonding interactions with Thr260, Ala256, Arg96, Phe78, Leu321, Tyr76 while compound **4 h** with the lone pair of -Cl have shown better interaction with the active site and were involved in H-bond interaction with THR 260. DNA binding study exhibited very good DNA-interaction (2.03×10^5 $Lmol^{-1}$) of compound **4b** with the hs-DNA. The results of DFT study and ADME investigations were accessed for the pharmacodynamics and pharmacokinetic properties of the synthesized molecules.

1. Introduction

In the past three decades, air and water pollution have increased at a rapid rate, which causes air and water-borne diseases and affecting human health adversely [1-3]. Fungal infection has increased rapidly and become one of the major concerns for human health [4]. Among several fungal species, Candida and Aspergillus are considered as the most common fungal pathogens which are responsible for the majority of fungal infections occurring worldwide [5, 6]. Azoles, polyenes and allylamines are commonly used antifungal drugs by targeting sterol 14α-demethylase, ergosterol, and β-1,3-glucan synthase, respectively [7]. The inhibition of lanosterol 14α-demethylase (CYP51) is gaining significant importance for developing antifungal drugs. The CYP51 protein is the main target for azoles and uses non-covalent ligand interactions to inhibit CYP51, which mediates membrane permeability and fluidity by demethylating the 14α-position of lanosterol to form ergosterol [7]. The thiazole containing heterocycles have attracted continuing interest because of their varied biological activities including antimicrobial [8], anticancer [9], antimalarial [10], antiviral [11] and CNS activity [12, 13]. Triazole ring has been reported as an important antifungal agent mainly because of its hydrogen bonding capability, moderate dipole character and high metabolic stability [14-17]. However, long time usage of antifungal drugs has directed to an increase in resistance to these drugs.

Therefore, there is an emergent need to synthesize new hybrid molecules with better binding affinity with drug target. The molecular hybridization approach is commonly used to synthesize new hybrid molecules that are supposed to be more biologically active than parent moieties. 1,2,3-Triazoles are well known for their broad range of biological applications [15, 18-21]. Similarly, the 4-HBT containing compounds are also known for their pharmacological properties [12]. 1,2,3-Triazoles and benzothiazole containing hybrid molecules exhibiting antimicrobial properties are not much explored [22, 23].

Although, both 4-HBT and triazoles are known for various pharmacological properties, only few reports of hybrid triazole which are composed of 4-HBT and triazole ring are present in the literature [24-27]. For example, Malic *et al.* [25] have synthesized triazoles with 4-amino phenylbenzothiazole derivative as azide unit and coumarin derivative as the alkyne part using $CuSO_4$/ Na-ascorbate catalyst in *t*-BuOH/ H_2O (1:1 v/v) solvent medium and under microwave conditions and explored antimicrobial activity. The same research group [26] have explored the two triazole hy-

* Corresponding author.
E-mail address: rktittaliitd@nitkkr.ac.in (R.K. Tittal).

https://doi.org/10.1016/j.molstruc.2021.131013
0022-2860/

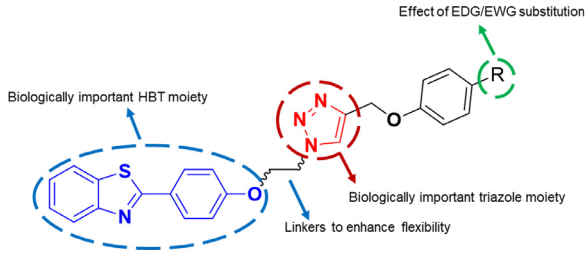

Fig. 1. Designing of 4-HBT linked 1,2,3- triazole derivatives.

brids with 4-aminophenylbenzothiazole unit with satisfactory yield and explored *in-vitro* antimicrobial activities. Rezki *et al.* [27] have synthesized benzothiazole linked triazole hybrids having alkoxy amide as the linker using $CuSO_4$/ Na-ascorbate as the catalyst and evaluated the antifungal and antibacterial activities. Kumbhare *et al.* [24] have synthesized benzothiazole based triazole hybrids by using CuI as the catalyst in dry THF conditions under ultrasound conditions and evaluated their anticancer activity. Although, the reported triazoles showed good anti-microbial and anticancer activities, but in some cases, synthesis was carried out under particular environment with dry organic solvents with no systematic DNA binding and detailed docking studies.

By keeping foregoing points in our mind mainly the well-known pharmacophore properties of triazole and benzothiazole, and also better binding capabilities of some of their hybrid molecules, herewith we have explored the synthesis and applications of 4-HBT linked 1,2,3-triazole hybrid molecules with varying alkyl linkers (Fig. 1). To the best of our knowledge, the 4-alkoxy phenyl benzothiazole linked 1,2,3-triazole hybrid molecules have not been synthesized earlier. The alkyl linkers are known to impart more flexibility to the geometry of the molecules and thus better conformation can be achieved to bind with the biological targets. The interactions of small molecules with DNA are well documented in the literature for determining their binding affinity with the DNA [28, 29]. Herein, we are presenting antifungal evaluation as well as DNA interactions of 4-HBT linked 1,2,3-triazole molecules. The molecular docking study [28] has finally provided information to understand the mechanism of their interaction and the type of non-covalent interactions involved.

2. Results and discussion

2.1. Chemistry

The desired 4-HBT linked 1,2,3-triazole hybrids were synthesized by the nucleophilic substitution reaction of different dibromo alkanes i.e., dibromo (ethane, propane and butane) with 4-HBT (**1**) using K_2CO_3 base as summarized in Scheme 1 to prepare different bromo alkoxy derivative **2a-c** in good yields. Thus, synthesized bromo alkoxy derivatives **2a-c** were subjected to react under CuAAC mediated (3 + 2) cycloaddition reaction with different alkyne derivatives **3a-e** via *insitu* formation of corresponding required organic azides to attain the desired 4-HBT linked 1,2,3-triazole derivatives **4a-o** in good to high yield (Scheme 1, **Table 1**).

The synthesized 4-HBT linked 1,2,3-triazole hybrid molecules were fully characterized by FT-IR, ^{1}H NMR, ^{13}C NMR, and ESI-MS data. For instance, the ^{1}H NMR spectrum of compound **4a** displayed two triplets in the aliphatic region at 4.54 ppm and 4.85 ppm corresponds to the hydrogens of an alkyl chain spacers, whereas, singlet at δ 5.17 ppm was assigned to the –OCH_2 linked to other side of triazole. The signals due to aromatic protons present in the 4-HBT skeleton and phenyl ring of propargyl moiety appeared in the corresponding aromatic region. Also, a characteristic singlet at δ value 8.35 ppm corresponds to a triazolyl proton to confirm the cycloaddition reaction. In the ^{13}C NMR spectrum, three characteristics carbon signals at δ 48.90, 60.85, 66.36 ppm were observed corresponding to the aliphatic carbon atoms present in 4a. i.e., two of ethyl chain as a linker and one of –OCH_2 group. In the FT-IR spectrum of the compound 4a, a characteristic absorption signal at 3143 cm^{-1} indicated the formation of triazole ring. The ESI-MS spectrum further supported the structure assigned to 4a as 2-(4-(2-(4-(phenoxymethyl)−1*H*-1,2,3-triazol-1-yl)ethoxy)phenyl)benzothiazole, showing molecular ion peak at *m/z* 429.14 which corresponds to its molecular formula $C_{24}H_{20}N_4O_2S$. A similar pattern of spectral peaks were obtained with all other triazole derivatives. The detailed spectral data of all the synthesized triazoles 4a-o is given in the Supplementary Information.

Table 1
Synthesis of 4-HBT linked 1,2,3-triazoles **4a-o**.[a]

S. No.	Compound	n	R	Time (h)	Yield (%)[b]
1.	**4a**	2	H	5	90
2.	**4b**	2	Me	5	94
3.	**4c**	2	Cl	6	85
4.	**4d**	2	COMe	7	87
5.	**4e**	2	NO_2	7	83
6.	**4f**	3	H	6	91
7.	**4g**	3	Me	5	93
8.	**4h**	3	Cl	6	83
9.	**4i**	3	COMe	6	85
10.	**4j**	3	NO_2	7	84
11.	**4k**	4	H	5	92
12.	**4l**	4	Me	6	90
13.	**4m**	4	Cl	6	86
14.	**4n**	4	COMe	7	85
15.	**4o**	4	NO_2	6	80

[a] 4-(n-(bromoalkoxy)phenyl)benzothiazoles **2a-c** (1 mmol), alkyne **3a-e** (1 mmol), NaN_3 (1.2 mmol), $CuSO_4 \bullet 5H_2O$ (10 mol%), Na-ascorbate (20 mol%), THF: H_2O (8:2 v/v ratio), 60 °C, 5–7 hrs.;.
[b] Yields refer to purification via column chromatography using ethyl acetate: hexane with increased polarity gradient.

Table 2
The antifungal activity data of synthesized 4-HBT linked 1,2,3-triazoles **4a-o**.

S. No.	Compound	n	R	Zone of inhibition (diameter in mm)	
				C. tropicalis	*A. terreus*
1.	**4a**	2	H	32.0	29.8
2.	**4b**	2	Me	30.6	27.6
3.	**4c**	2	Cl	31.0	27.0
4.	**4d**	2	COMe	27.0	26.0
5.	**4e**	2	NO_2	14.0	22.5
6.	**4f**	3	H	32.6	30.2
7.	**4g**	3	Me	31.1	29.3
8.	**4h**	3	Cl	33.1	30.5
9.	**4i**	3	COMe	14.0	24.0
10.	**4j**	3	NO_2	28.2	26.5
11.	**4k**	4	H	29.5	28.7
12.	**4l**	4	Me	30.2	29.0
13.	**4m**	4	Cl	29.0	28.1
14.	**4n**	4	COMe	21.5	27.0
15.	**4o**	4	NO_2	29.3	28.0
16.	DMSO	–	–	00	00
17.	Fluconazole	–	–	21.0	19.0

Evaluation of antifungal activity: The antifungal evaluation of all the synthesized 1,2,3-triazoles **4a-o** was carried out against fungal strains *C. tropicalis* MTCC 184, and *A. terreus* MTCC 1325 by agar well diffusion method. Here, DMSO and the fluconazole were used as negative control and standard reference, respectively. The diameter of zone of inhibition (ZOI) of all the 1,2,3-triazoles **4a-o** was measured (in mm) as mentioned in **Table 2**.

The antifungal activity results indicated that most of the synthesized 4-HBT linked 1,2,3-triazoles reflected good antifungal activity against *C. tropicalis* except **4e** and **4i**. Overall, compound **4h**

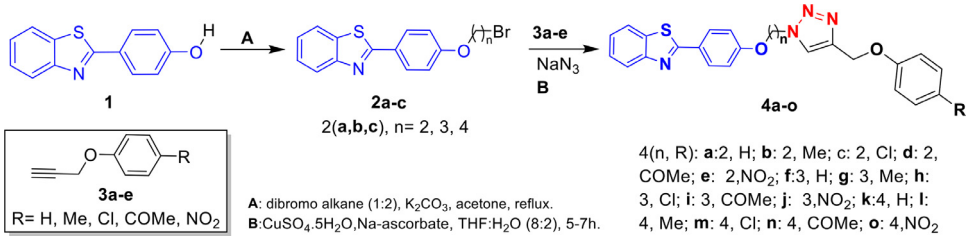

Scheme 1. . Synthesis of 4-HBT linked triazole hybrid molecule **4a-o**.

Table 3
Docking results of 4-HBT linked 1,2,3-triazole **4a-o** and their interactions with 14α- demethylase lanosterol enzyme.

Compound	BE[a]	run	IME[b]	IE[c]	TorE[d]	VdwE[e]	EE[f]	Ki[g](pM)
4a	−14.53	3rd	−14.81	−2.34	2.09	−14.62	−0.19	22.35
4b	−13.32	4th	−13.39	−3.05	2.39	−13.44	0.05	171.85
4c	−13.61	4th	−14.15	−2.57	2.39	−14.26	0.10	105.71
4d	−12.43	3rd	−13.80	−2.12	2.68	−13.65	−0.15	777.31
4e	−11.17	10th	−12.35	−2.31	2.68	−13.18	0.84	6470
4f	−14.76	7th	−15.19	−2.96	2.68	−15.15	−0.04	15.14
4g	−14.25	4th	−14.43	−3.23	2.68	−14.25	−0.17	35.66
4h	−15.07	2nd	−15.46	−3.01	2.68	−15.32	−0.14	08.95
4i	−12.17	7th	−13.78	−2.17	2.98	−13.77	−0.02	1200
4j	−13.13	10th	−15.03	−1.86	2.98	−15.68	0.65	235.66
4k	−13.70	3rd	−15.10	−2.38	2.98	−15.13	0.03	91.01
4l	−13.89	5th	−15.05	−2.63	2.98	−14.80	−0.25	65.84
4m	−13.08	2nd	−14.32	−2.56	2.98	−14.49	0.17	257.64
4n	−12.10	1st	−14.93	−1.33	3.28	−14.87	−0.06	1350
4o	−12.76	5th	−14.03	−2.88	3.28	−14.60	0.57	439.86
Fluconazole	−8.26	5th	−8.82	−2.18	1.79	−8.77	−0.06	886.18nM

[a] : BE = Binding energy (kcal/mol),.
[b] : IME= Intermolecular energy (kcal/mol),.
[c] : IE= Internal energy (kcal/mol),.
[d] : TE= Torsional energy (kcal/mol),.
[e] : VdwE = Vander waal Energy vdW+*H*-bond+desolv energy (kcal/mol),.
[f] : EE= Electrostatic energy (kcal/mol),.
[g] : Ki= Inhibition constant (pM).

($n = 3$ and R = Cl) revealed better activity against both the fungal strains among all the synthesized 1,2,3-triazoles and unsubstituted compounds (**4a**, **4f**, **4k**) showed good activity against both the strains. The structure-activity relationship analysis revealed that compounds containing electron withdrawing substitution at the para position of phenyl ring are comparatively lesser antifungal active than the compounds containing electron-donating substitution at the para position.

2.2. Molecular docking

From the antifungal activity experiments, we have found that synthesized triazoles showed significant inhibition of the fungal activity. Azoles act as antifungal agent mainly by inhibiting the cytochrome 450 dependent conversion of Lanosterol to Ergosterol which is a major membrane sterol of fungi. Triazoles act as 14α-demethylase inhibitor and so inhibit the Ergosterol synthesis [30]. Therefore, to scrutinize the mode of interaction of synthesized triazoles 4a-o into active sites of 14α-demethylase, molecular docking studies were performed. For this purpose, the active site of enzyme 14α-demethylase (PDBID: **1EA1**) was considered for molecular docking of synthesized triazoles and calculations were performed using software Autodock 4.0 [31]. From docking results as presented in Table 3, it was observed that some of the triazoles showed effective H-bond interaction with the active site of 14α-demethylase. To compare the interactions of all the synthesized triazole with the standard, fluconazole was also docked at the same active site of the enzyme. The results revealed that most of the triazoles understudy shown better free energy of binding than the standard fluconazole. While compound **4d**, **4e**, **4i**, and **4j** having electron withdrawing groups (-NO_2 and -COMe) at the para position shown less effective interaction as compared to the compounds **4b**, **4g**, and **4l** which have electron donating groups at the para position.

It was observed that among all the compounds the triazoles having -Cl group as substituent have shown better interaction with the active site. In compound 4 h, the lone pair of chlorine were involved in H-bond interaction with THR260 present in the active site of the enzyme as represented in Fig. 2. The binding modes for rest of compounds (**4a**-**g**, and **4i**-**o**) in the active site of cytochrome 450 14α- demethylase enzyme are mentioned in **Figures SI-64** to **SI-78**. Further, all 1,2,3-triazole hybrids exhibited strong H-bonding interactions with Thr260, Ala256, Arg96, Phe78, Leu321, Tyr76 as represented in Table 4, thereby stabilizing the enzyme-inhibitor complex at the active site.

2.3. DNA binding studies

UV–visible spectroscopy is one of the most widely used technique to evaluate the interactions of small molecules with DNA [32, 33]. When any molecule interacts with DNA there is a subsequent change in the absorption spectrum in the form of hypochromic or hyperchromic shift. Generally, more is the shift in absorbance more will be an interaction between a compound and DNA. Among all the synthesized compounds **4b** showed better interaction with the hs-DNA. The UV absorbance spectrum of **4b** with increasing concentration of hs-DNA is shown in **Fig. 3**. Without hs-DNA, **4b** molecule showed a broad absorption band around 320 nm, which corresponds to the core benzothiazole structure [34]. However, hs-DNA has a characteristic peak at 260 nm. By

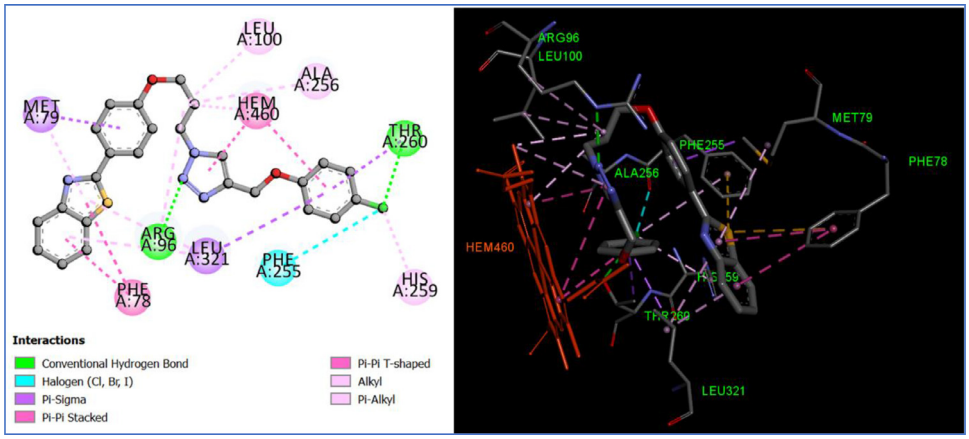

Fig. 2. 2D and 3D binding interactions representation of **4h** in active site of cytochrome 450 14α-sterol demethylase enzyme CYP51 (PDBID: **1EA1**).

Table 4
The binding energies and interactions obtained from the docking results of **4a-o**.

Ligand	B.E. (kcal/mol)	Interactions (active site-ligand)
4a	−14.51	Hem460, THR260, ALA256, ARG96, PHE78, LEU321, TYR76
4b	−13.32	Hem460, LEU100, MET99, PHE78, ALA256, LEU321, MET79, TYR76
4c	−13.61	Hem460, PHE78, TYR76, LEU321, MET79, LEU100, ALA256, PHE255, HIS259, THR260
4d	−12.43	Hem460, HIS259, LEU321, PHE78, TYR76, PHE255, MET79, ALA256, ARG96, LEU100, MET99
4e	−11.17	Hem460, LEU100, ALA256, PHE83, MET79, PHE255, THR260, LEU321, TYR76
4f	−14.76	Hem460, HIS259, PHE78, LEU321, MET79, THR260, ALA256, LEU100, ARG96
4g	−14.25	Hem460, ARG96, MET99, LEU100, PHE255, MET79, ALA256, LEU321, PHE78, TYR76, HIS259
4h	−15.07	Hem460, MET79, PHE78, ARG96, LEU321, PHE255, LEU100, ALA256, THR260, HIS259, LEU321
4i	−12.17	Hem460, ARG96, PHE83, MET99, LEU100, ALA256, MET79, THR260, HIS259, LEU321, PHE78, TYR76
4j	−13.13	Hem460, HIS259, HIS258, THR260, ALA256, ARG96, LEU100, MET79, TYR76, PHE78, LEU321, TYR76
4k	−13.70	Hem460, PHE78, MET79, LEU321, TYR76, ARG96, LEU100, ALA256, THR260, PHE83
4l	−13.89	Hem460, LEU321, PHE256, PHE78, TYR76, MET79, ARG96, ALA256, LEU100, MET99, THR260
4m	−13.08	Hem460, THR260, HIS259, ALA256, LEU321, MET79, TYR76, PHE78, LEU100, ARG96
4n	−12.10	Hem460, PHE78, MET79, TYR76, LEU321, ALA256, LEU100, GLN72, ARG96, ALA256
4o	−12.76	Hem460, THR260, HIS259, ARG96, ALA256, LEU100, LEU321, MET79, PHE255, TYR76, PHE78

keeping a fixed concentration compound **4b** in cuvette the hs-DNA added and hypochromic shift was observed. The change in absorption spectra indicated the **4b**-DNA complex formation. The absorbance titration of the other remaining triazoles with the hs-DNA were carried out under similar experimental conditions and their respective binding constant plots are given in **Figures SI-52 to SI-63** in supplementary information file and calculated binding constant values are shown in **Table 5**. Further, the DNA association ability was calculated quantitatively in the form of intrinsic binding constant (K_b) by the following reported equation [35]:

$$\frac{1}{A_0 - A} = \frac{1}{A_0} + \frac{1}{k * A_0 * C_{DNA}}$$

Whereas "A_0" is initial absorbance, "A" denotes final absorbance, "C_{DNA}" corresponds to the concentration of DNA and "*k*" is the binding constant.

To understand their interaction molecular docking was performed and **4a-o** docked in the active site of DNA dodecamer (PDBID: **1BNA**) as shown in **Table 6**. Also, to further get the closer information, various binding interactions of all synthesized compounds were evaluated and their 2D and 3D representations are presented in **Figures SI-52 to SI-63**. For easy reference compounds **4b** and **4 g** are shown in **Fig. 4**and **5**, which showed high binding constant values. It was observed that **4b** have shown effective interaction with the active site and binds to the groove region of the DNA as shown in **Fig. 6** with the binding energy −7.39 kcal/mol.

Table 5
The binding constant (K_b) and%Hypochromism (H%) results of synthesized 1,2,3- triazole hybrid **4a-o** with hs-DNA.

S. No.	Compound	n	R	Absorbance free	Absorbance bound	H%[a]	K_b ($Lmol^{-1}$)>[b] × 10^5
1.	**4a**	2	H	0.2291	0.1768	22.8	0.95
2.	**4b**	2	Me	0.3462	0.2844	17.8	2.03
3.	**4c**	2	Cl	0.2403	0.2069	13.8	0.28
4.	**4d**	2	COMe	0.2100	0.1537	26.8	1.61
5.	**4e**	2	NO_2	0.1624	0.1482	8.74	0.31
6.	**4f**	3	H	0.3731	0.3182	14.7	0.90
7.	**4g**	3	Me	0.1655	0.1339	19.0	1.97
8.	**4h**	3	Cl	0.3017	0.2795	7.35	0.56
9.	**4i**	3	COMe	0.1925	0.1694	12.0	0.96
10.	**4j**	3	NO_2	0.2692	0.2389	11.2	1.59
11.	**4k**	4	H	0.3807	0.3424	10.0	0.93
12.	**4l**	4	Me	0.2509	0.2328	7.21	0.28
13.	**4m**	4	Cl	0.4802	0.4357	9.26	0.68
14.	**4n**	4	COMe	0.1172	0.1113	0.59	0.05
15.	**4o**	4	NO_2	0.3258	0.2991	8.19	0.42

[a] : H% (%hypochromism) = $[(A_f - A_b)/A_f)] \times 100$, Where A_f and A_b represent the absorbance of free and bound compounds,.
[b] : K_b=Intrinsic binding constant.

2.4. ADME prediction

In the last two decades, *in-silico* studies of biological applications have attracted the attention of scientists [36]. For instance, *in-silico* ADME investigations are found to be a helpful and promising technique to choose a particular bio-active compound from the library of compounds [37-39]. This investigation usually helps to understand and minimize the risk of the drug in human beings at

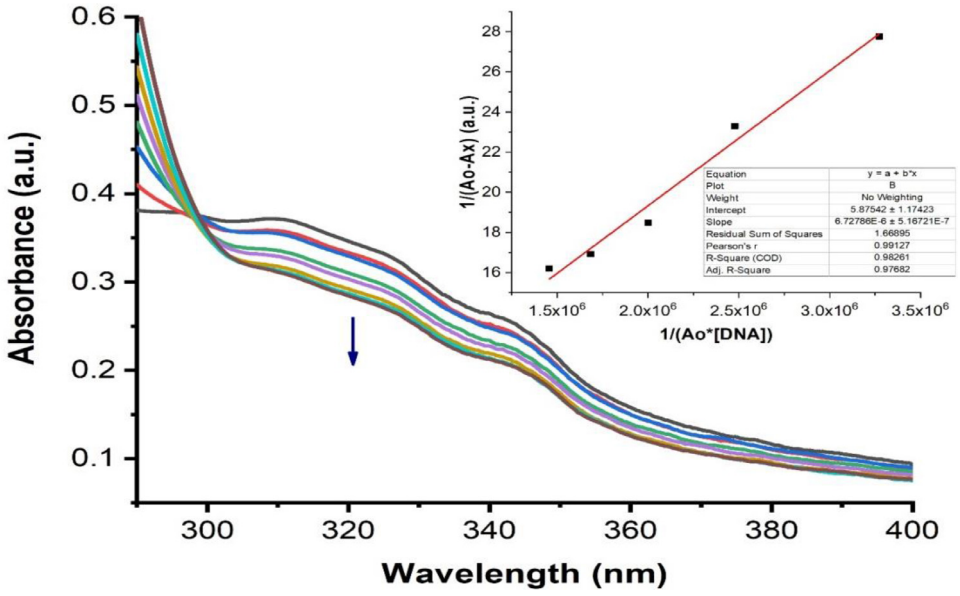

Fig. 3. Compound **4b** vs hs-DNA (0 - 2.7 × 10^{-6} M) systematic absorption titration (arrow indicate change in absorbance); Linear plot for calculating binding constant (given in inset).

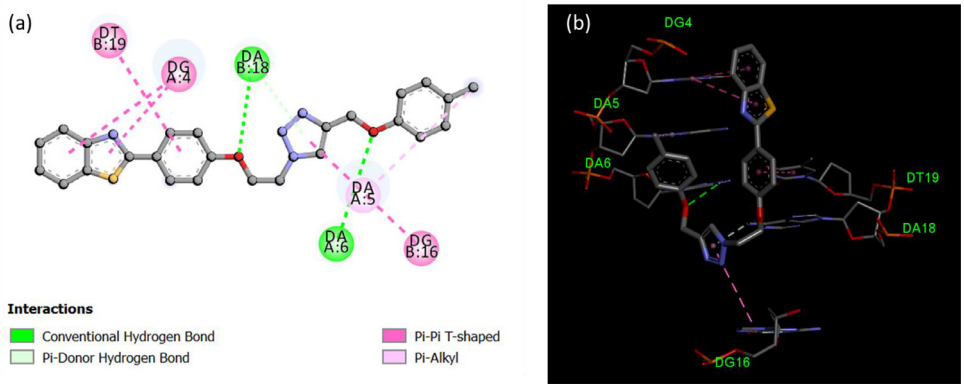

Fig. 4. 2D (a) and 3D (b) binding interactions representation of **4b** with DNA residue.

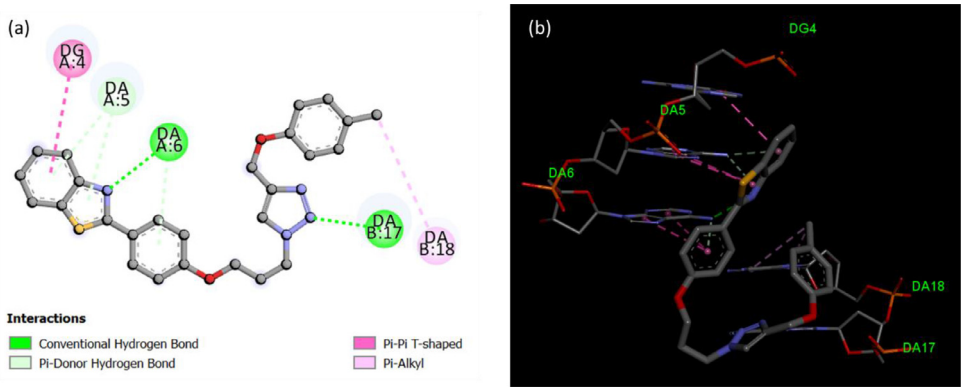

Fig. 5. 2D (a) and 3D (b) binding interactions representation of **4g** with DNA residue.

a later stage. It is expected that for desired *in-vivo* activity, equilibrium between pharmacodynamic and pharmacokinetic properties is needed. Various parameters from ADME studies provide detailed information related to brain penetration, oral bioavailability and clearance after drug dosage. Including these methods of virtual screening, other parameters such as drug-likeness score, human intestinal absorption, partition coefficient, polar surface area and cell permeability can be studied. The *in-silico* investigations of synthesized triazoles **4a-o** were performed to evaluate the physiochemical parameters such as MLogP, HBA, MR, RB, HA, MW, TPSA, HBD, using SwissADME software [40] as presented in **Table 7**. A molecule is likely to be developed as an orally active drug that should obey four or more points as mentioned in the Lipinski *rule of five* [41]. As per the Lipinski rule, any molecule could be con-

Table 6
The binding energies of **4a-o** docked in the active site of DNA dodecamer (PDBID: **1BNA**).

S. No.	Compound	n	R	B.E. (kcal/mol)
1.	**4a**	2	H	−7.42
2.	**4b**	2	Me	−7.39
3.	**4c**	2	Cl	−7.12
4.	**4d**	2	COMe	−7.48
5.	**4e**	2	NO_2	−6.43
6.	**4f**	3	H	−7.22
7.	**4g**	3	Me	−7.29
8.	**4h**	3	Cl	−7.17
9.	**4i**	3	COMe	−7.05
10.	**4j**	3	NO_2	−6.54
11.	**4k**	4	H	−6.59
12.	**4l**	4	Me	−6.81
13.	**4m**	4	Cl	−7.21
14.	**4n**	4	COMe	−6.96
15.	**4o**	4	NO_2	−5.51

sidered suitable as an oral drug which agrees with five important points: a) Molecular weight ≤ 500, b) MLog P ≤ 5, c) Number of hydrogen bond acceptor ≤ 10 and d) Number of hydrogen bond donor ≤ 5. Here, the number of rotatable bonds represents the molecular flexibility and plays an important role in oral bioavailability; if the molecule is flexible, that indicate the drug is less orally active. It was observed that most of the synthesized compounds have all the parameters in the expected range.

Drug likeness score was calculated using molsoft [42] and the bioactivity score result indicated in **Table 8** wherein most of the compounds were found in the acceptable range. The pharmacokinetic parameters related to effective nature of drug in the body such as PPB predictions, BBB penetration, Plasma protein binding, Pgb inhibition and human intestinal absorption were evaluated using PreADMET software [43-45] available online (https://preadmet.bmdrc.kr/) as shown in **Table 9**. PreADME studies have also been used to evaluate useful parameters related to its effective nature in the body. PPB analysis was carried out based on the criteria- a) with a score more than 90%: chemicals strongly binds and b) a score less than 90%, chemicals weakly bind. It is evident

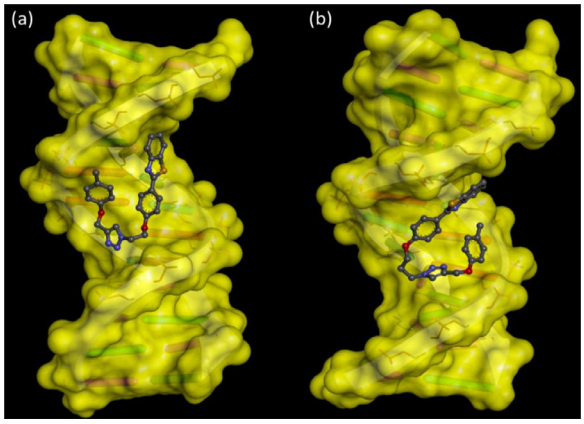

Fig. 6. Docked pose of **4b**(a), and **4g**(b) in the groove region of DNA (PDBID: **1BNA**).

Table 8
The bioactivity score by Molinspiration [46] property calculator toolkit.

S. No.	Compound	GPCR[a]	ICM[b]	KI[c]	NR[d]	PI[e]	EI[f]
1.	**4a**	−0.11	−0.43	0.12	−0.20	−0.21	0.08
2.	**4b**	−0.14	−0.47	0.08	−0.22	−0.25	0.03
3.	**4c**	−0.11	−0.42	0.10	−0.22	−0.24	0.05
4.	**4d**	−0.16	−0.46	−0.02	−0.25	−0.25	0.01
5.	**4e**	−0.22	−0.43	−0.00	−0.27	−0.30	−0.02
6.	**4f**	−0.08	−0.34	0.12	−0.18	−0.13	0.07
7.	**4g**	−0.11	−0.39	0.08	−0.20	−0.17	0.02
8.	**4h**	−0.08	−0.34	0.10	−0.20	−0.16	0.04
9.	**4i**	−0.13	−0.39	−0.02	−0.23	−0.18	0.00
10.	**4j**	−0.19	−0.37	0.00	−0.25	−0.23	−0.03
11.	**4k**	−0.04	−0.30	0.10	−0.20	−0.12	0.10
12.	**4l**	−0.07	−0.35	0.06	−0.21	−0.16	0.05
13.	**4m**	−0.04	−0.30	0.08	−0.21	−0.15	0.07
14.	**4n**	−0.09	−0.37	−0.03	−0.24	−0.17	0.03
15.	**4o**	−0.15	−0.35	−0.01	−0.26	−0.22	0.00

[a] GPCR= GPCR ligand;.
[b] ICM= Ion channel modulator;.
[c] KI= Kinase inhibitor;.
[d] NR= Nuclear receptor ligand;.
[e] PI= Protease inhibitor;.
[f] EI= Enzyme inhibitor.

Table 7
The *in-silico* ADME prediction and drug-likeness model score.

Compound **Rule**	MR[a] –	TPSA[b] –	RB[c] –	HA[d] –	MW[e] ≤500	MLogP[f] ≤ 5	HBA[g] ≤10	HBD[h] ≤5	Lipinski violations[i] ≤ 1	Drug-likeness[j] –
4a	121.70	90.30	8	31	428.51	3.37	5	0	0	0.07
4b	126.66	90.30	8	32	442.53	3.58	5	0	0	0.12
4c	126.71	90.30	8	32	462.95	3.85	5	0	0	0.52
4d	131.89	107.37	9	34	470.54	2.91	6	0	0	0.02
4e	130.52	136.12	9	34	473.50	3.23	7	0	0	−0.37
4f	126.50	90.30	9	32	442.53	3.58	5	0	0	0.13
4g	131.47	90.30	9	33	456.56	3.78	5	0	0	0.16
4h	131.51	90.30	9	33	476.98	4.05	5	0	0	0.54
4i	136.70	107.37	10	35	484.57	3.12	6	0	0	0.09
4j	135.33	136.12	10	35	487.53	3.44	7	0	0	−0.32
4k	131.31	90.30	10	33	456.56	3.78	5	0	0	0.19
4l	136.28	90.30	10	34	470.59	3.98	5	0	0	0.21
4m	136.32	90.30	10	34	491.00	4.15	5	0	1	0.58
4n	141.51	107.37	11	36	498.60	3.31	6	0	0	0.14
4o	140.13	136.12	11	36	501.56	3.65	7	0	1	−0.29

[a] MR= Molar refractivity;.
[b] TPSA= Topographical polar surface area;.
[c] RB= Number of rotatable bonds;.
[d] HA= No. of heavy atoms;.
[e] MW= Molecular weight;.
[f] MlogP= Lipophilicity;.
[g] HBA= No. of hydrogen bond acceptors;.
[h] HBD= No. of hydrogen bond donors;.
[i] Number of violations;.
[j] Drug-likeness model score.

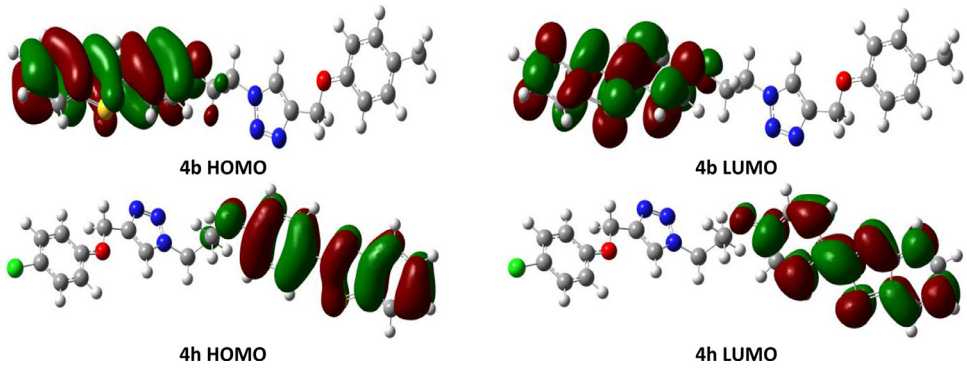

Fig. 7. HOMO and LUMO distributions at the ground states of **4b** and **4 h** molecules.

Table 9
Pharmacokinetic parameter calculated using PreADMET.

S. No.	Compound	BBB[a]	HIA[b]	Caco2[c]	SP[d]	MDCK[e]	PPB[f]
1.	**4a**	0.048	97.752	24.181	−2.880	81.846	98.619
2.	**4b**	0.039	97.702	24.727	−2.848	72.823	96.538
3.	**4c**	0.029	97.676	50.761	−2.924	68.177	98.114
4.	**4d**	0.044	98.500	24.370	−3.036	14.514	94.832
5.	**4e**	0.355	99.810	17.962	−2.771	1.5375	97.312
6.	**4f**	0.216	97.702	24.956	−2.805	27.846	99.832
7.	**4g**	0.170	97.673	25.567	−2.780	30.748	97.249
8.	**4h**	0.098	97.701	51.955	−2.850	23.962	99.457
9.	**4i**	0.121	98.330	25.435	−2.961	0.488	95.331
10.	**4j**	0.440	99.975	19.334	−2.689	0.163	97.857
11.	**4k**	0.061	97.673	23.841	−2.617	28.423	99.879
12.	**4l**	0.050	97.661	24.304	−2.598	32.944	98.179
13.	**4m**	0.038	97.733	50.844	−2.659	27.26	99.443
14.	**4n**	0.045	98.181	24.216	−2.764	0.519	96.263
15.	**4o**	0.628	100.00	19.965	−2.504	0.154	98.054

[a] BBB= blood-brain barrier penetration;.
[b] HIA= Human intestinal absorption (%);.
[c] Caco2 cell permeability;.
[d] SP= Skin permeability;.
[e] MDCK cell permeability;.
[f] PPB= Plasma protein binding (%).

from the data shown in **Table 9**, all the synthesized compounds strongly bound to plasma protein. Another important parameter, blood-brain barrier (BBB) penetration obeys the criteria [43] i.e. a) High absorption to CNS for BB>2.0; b) Moderate absorption to CNS for BB between 2.0–0.1; and c) low absorption to CNS for BB<0.1. The results obtained from BBB studies showed that **4e, 4f, 4 g**, and **4i** may have moderately acceptable absorption to CNS, while others show low absorption. Further, human intestinal absorption (HIA) results were evaluated by following these points: a) HIA between 0% and 20% (Poorly absorbed) b) HIA between 20% and 70% (Moderately absorbed) and c) HIA between 70% and 100% (high absorbed). For this parameter, all the compounds have shown well human intestinal absorption properties. Therefore, almost all the synthesized triazoles have well to better PreADME results and have the potential for active biological applicability.

2.5. DFT study

The study of frontier molecular orbitals (FMO) through the density functional theory (DFT) provided us a very useful tool to evaluate the important reactivity parameters in order to efficiently design various classes of drugs with the help of available data or library of various related chemical compounds [42, 47, 48]. Molecular geometry of all the synthesized 4-HBT linked 1,2,3-triazole molecules **4a**-**o** were optimized with the help of Gaussian 09 program using B3LYP and 6–311G(d,p) level and basis set, respectively [46]. The optimized structures of all the synthesized triazoles **4a**-**o** were also verified to be local minima, without any imaginary frequencies. In general the lower energy orbitals that have empty molecular orbital or also called lowest unoccupied molecular orbital (LUMO) of the acceptor molecules generally accepts the electrons from the higher energy orbitals that have filled molecular orbitals or also called highest occupied molecular orbital (HOMO). The energy parameters of the frontier orbitals like energy gap, chemical potential and the chemical hardness are represented by $\Delta E_{LUMO-HOMO}$, μ, and η, respectively and were computed by using Koopmans' theorem [49]. However, the electrophilicity index represented by ω was calculated by using Robert G. Parr approximation [50-52]. The three relations for μ, η, and ω (i - iii) as detailed in SI file and the results are summarized in **Table 10**. The chemical hardness (η) of the compound can be computed with the help of mean value of HOMO-LUMO energy gap that shows reactivity of the compound. The higher values of η show hardness of the molecules while, lower values show softness. The more energy gap needs high excitation energy to cross or reach the excitation state and hence, hard the molecule to react as compared to the soft molecules that possesses lower energy gap. The computed values of the chemical hardness showed following decreasing trend of chemical hardness of 4-HBT linked 1,2,3-triazoles **4a**-**o** molecules: (Harder) **4b**>**4a**≈**4c**-***d***>**4f**-**g** ≈**4i**>**4k**-***n***>**4h**>**4e**>**4j**>**4o** (Softer)

The complete details on the FMOs distribution pattern of 4-HBT linked 1,2,3-triazoles **4a**-**o** are given in **Figure SI-76**. For ready reference, the FMOs of **4h** and **4b** most promising compounds on the basis of antifungal activity and molecular docking results, respec-

Table 10
Chemical reactivity parameters ($\Delta E_{LUMO-HOMO}$, μ, η, and ω) in eV of **4a-o** computed by DFT (B3LYP/6–311G(d,p) level).

Compound	Parameters (eV)					
	E_{HOMO}	E_{LUMO}	$E_{LUMO-HOMO}$	μ	η	ω
4a	−6.05	−1.73	4.32	−3.89	2.16	3.51
4b	−6.06	−1.73	4.33	−3.90	2.17	3.50
4c	−6.09	−1.77	4.32	−3.93	2.16	3.57
4d	−6.10	−1.78	4.32	−3.94	2.16	3.59
4e	−6.15	−2.43	3.72	−4.29	1.86	4.94
4f	−6.03	−1.72	4.31	−3.87	2.15	3.48
4g	−6.02	−1.72	4.31	−3.87	2.15	3.48
4h	−6.02	−1.73	4.29	−3.87	2.14	3.49
4i	−6.06	−1.75	4.31	−3.90	2.16	3.53
4j	−6.10	−2.44	3.66	−4.27	1.83	4.99
4k	−5.98	−1.67	4.30	−3.82	2.15	3.40
4l	−5.97	−1.67	4.30	−3.82	2.15	3.40
4m	−6.00	−1.70	4.30	−3.85	2.15	3.44
4n	−6.00	−1.70	4.30	−3.85	2.15	3.44
4o	−6.04	−2.40	3.64	−4.22	1.82	4.88

tively, are shown in **Fig. 7**. Considering the decreasing trend of the chemical hardness and the relative positions of the **4h** and **4b**, it revealed that the high reactivity of **4h** is also supported by the DFT results.

3. Conclusion

Bioactive 1,2,3-triazoles, and 4-HBT linked with varying alkyl spacers were synthesized and fully characterized. All the synthesized molecules were evaluated for *in-vitro* antifungal activity wherein compound **4h** showed better activity against both *C. tropicalis* and *A. terreus* fungal strains. In DNA binding studies, compound **4b** exhibited very good interaction with the hs-DNA. Molecular docking results showed compound **4h** with the lone pair of chlorine have shown better interaction with the active site and were involved in H-bond interaction with Thr260. Also, DFT and ADME predictions for the pharmacodynamics and pharmacokinetic properties revealed the medicinal potential of these molecules for further investigations to get some hybrid lead.

4. Experimental section

General Information: ^{1}H NMR and ^{13}C NMR spectra were recorded on Bruker Avance 500 MHz spectrometer, whereas ^{13}C NMR spectra were acquired on the same instrument at 125 MHz using tetramethylsilane (TMS) as the internal standard. ESI-MS spectra were recorded on a WATERS XEVO G2-XS QTOF instrument. FT-IR (Fourier transform-infrared) analysis was carried out on Shimadzu IR-Instrument using anhydrous KBr pellets. The column chromatography with silica gel of 100–200 mesh size was purchased from Avra Chemicals Limited, chemicals and solvents used were of analytical grade. The open tube capillary method was used for determining melting points of the synthesized compounds and is uncorrected.

4.1. Pharmacological study

4.1.1. Antifungal study

The antifungal activity was performed by the agar-well diffusion method [53-55]. DMSO was taken as the negative control and the Fluconazole as a standard reference. The tested compounds were dissolved in DMSO to prepare a stock solution of concentration 50 µg mL^{-1}. The diameter of the inhibition zone (DIZ) around each well caused by the 50 µL of the test sample was measured in mm after the overnight incubation at 37 °C to determine the activity of that compound and compared with the reference compound.

DNA binding studies: The *invitro* DNA binding studies were performed on the Thermofisher Scientific EVOLUTION 300 UV–vis spectrophotometer. The hs-DNA (degraded free acid) was purchased from SRL (Sisco Research Laboratories Pvt. Ltd.). Absorption spectra were recorded ranging from 240 nm to 450 nm with increasing concentration of hs-DNA (from 0 to 2.7 × 10^{-6} M). The 5 mM Tris–HCl/50 mM NaCl buffered medium was used for preparing hs-DNA stock solution and protein-free nature of DNA was confirmed by ratio obtained (1.8–1.9) of UV absorbance at 260 and 280 nm.

Molecular docking study: The crystal structure of the DNA dodecamer (PDBID: **1BNA**) of sequenced $(CGCGAATTCGCG)_2$ and crystal structure of target enzyme Cytochrome P450 14α-sterol demethylase (CYP51) from Mycobacterium tuberculosis in complex with fluconazole (PDBID:**1EA1**) was downloaded in pdb format from the RCSB protein data bank (www.rcsb.org). The 3D structures of the ligand were drawn in CHEMSKETCH (www.acdlabs.com) and energy minimization was done using SPDBV software. Ligand preparation and receptor preparation was done using AutoDockTools-1.5.6 software. Gasteiger charges were added, water was removed and polar hydrogens were added. Ligand and receptor were saved in pdbqt format using AutoDockTools-1.5.6 software. Docking was performed by using the AutoDock 4.0 program open-source molecular docking software. Visualization of the results was done using Discovery studio visualizer. [56]

4.1.2. General procedure for the synthesis of triazole derivatives (4a-o) [33]

In a 100 mL round bottom flask, *2-(4-(2-bromoethoxy)phenyl)benzothiazole* **2a** (1.0 mmol) was taken in 20 mL of THF: H_2O (8:2, v/v) as solvent. To this solution sodium azide (1.2 mmol) was added and the reaction mixture stirred for a while at RT and further propargyl derivative **3a** (1 mmol) along with $CuSO_4$•$5H_2O$ (10 mol%) and Na-ascorbate (20 mol%) were added and the reaction mixture was heated at 60 °C for 5 h. After the completion of the reaction as indicated by TLC, THF was evaporated under reduced pressure and deionized water (30 mL) was added and ethyl acetate was used for extracting the compound in the organic phase. The organic layer was then washed with ammonia solution, dried over sodium sulfate and evaporated over rotary to get the desired product. The crude was then further purified by passing through a short band of silica column as the stationary phase using ethyl acetate: hexane as mobile phase using increased polarity gradient and obtained **4a-o** in good to better yields.

2-(4-(2-(4-(phenoxymethyl)−1H-1,2,3-triazol-1-yl)ethoxy) phenyl)benzothiazole (**4a**): Off white solid, yield: 90%, m.p. 132–134 °C. FT IR (KBr, ν_{max}/cm^{-1}): 3143, 3064, 2964, 2873, 1600, 1487, 1307, 1244 cm^{-1}. ^{1}H NMR (500 MHz, DMSO–d_6): δ = 4.54 (t, J = 5.08 Hz, 2H, CH_2), 4.85 (t, J = 5.04 Hz, 2H, CH_2), 5.17 (s, 2H, CH_2), 6.96 (m, 1H), 7.05 (dd, J = 8.27, 1.49 Hz, 2H), 7.11 (m, 2H), 7.30 (m, 2H, Ar-H), 7.43 (m, 1H, Ar-H), 7.53 (m, 1H, Ar-H), 8.02 (m, 3H, 8.11 (dd, J = 7.98, 0.59 Hz, 1H, Ar-H), 8.35 (s, 1H, triazole-CH); ^{13}C NMR (125 MHz, DMSO–d_6): δ = 48.90, 60.85, 66.36, 114.58, 115.28, 120.74, 122.13, 122.44, 125.04, 125.08, 125.96, 126.46, 128.80, 129.41, 134.19, 142.74, 153.57, 157.95, 160.22, 166.81. ESI-MS $[M + H]^+$: m/z cal. for $C_{24}H_{21}N_4O_2S$ is 429.14, found 429.14.

2-(4-(2-(4-((p-tolyloxy)methyl)−1H-1,2,3-triazol-1-yl)ethoxy) phenyl)benzothiazole **(4b)**: Off-White solid, yield: 94%, m.p. 140–142 °C. FT IR (KBr, ν_{max}/cm^{-1}): 3072, 2912, 2868, 1606, 1512, 1483, 1244, 1172 cm^{-1}. ^{1}H NMR (500 MHz, DMSO–d_6): δ = 2.23 (s, 3H, CH_3), 4.53 (t, J = 5.05 Hz, 2H, CH_2), 4.84 (t, J = 5.05 Hz, 2H, CH_2), 5.12 (s, 2H, CH_2), 6.93 (m, 2H), 7.10 (m, 4H), 7.43 (td, J = 7.65, 7.20, 1.17 Hz, 1H, Ar-H), 7.53 (m, 1H, Ar-H), 8.02 (dd,

J = 8.68, 1.97 Hz, 3H, Ar-H), 8.11 (d, J = 7.15 Hz, 1H), 8.32 (s, 1H, triazole-CH); ^{13}C NMR (125 MHz, DMSO–d_6): δ = 19.98, 48.87, 60.92, 66.35, 114.44, 115.27, 122.12, 122.43, 124.96, 125.07, 125.94, 126.45, 128.78, 129.37, 129.72, 134.17, 142.86, 153.56, 155.81, 160.21, 166.79. ESI-MS $[M + H]^+$: *m/z* cal. for $C_{25}H_{23}N_4O_2S$ is 443.15, found 443.15.

2-(4-(2-(4-((4-chlorophenoxy)methyl)−1H-1,2,3-triazol-1-yl)ethoxy)phenyl)benzothiazole (**4c**): Off-white solid, Yield: 85%, m.p. 130–132 °C. FT-IR (KBr, ν_{max}/cm^{-1}) = 3088, 2941, 2875, 1606, 1490, 1240 cm^{-1}. ^{1}H NMR (500 MHz, DMSO–d_6): δ = 4.53 (t, J = 5.06 Hz, 2H, CH_2), 4.85 (t, J = 5.01 Hz, 2H, CH_2), 5.18 (s, 2H, CH_2), 7.09 (dd, J = 11.9 and 8.99 Hz, 4H, Ar-H),7.34 (m, 2H, Ar-H), 7.43 (td, J = 7.69,7.28, 1.15 Hz, 1H, Ar-H), 7.53 (ddd, J = 8.29, 7.25, 1.24 Hz, 1H, Ar-H), 8.03 (m, 3H, Ar-H), 8.11 (d, J = 7.50 Hz, 1H, Ar-H), 8.35 (s, 1H, triazole-CH); ^{13}C NMR (125 MHz, DMSO–d_6): δ = 48.92, 61.25, 66.36, 115.27, 116.44, 122.13, 122.45, 124.49, 125.08, 125.20, 125.97, 126.46, 128.80, 129.16, 134.20, 142.39, 153.57, 156.76, 160.21, 166.81. ESI-MS (*m/z*) $C_{24}H_{20}ClN_4O_2S$: Calculated $[M + H]^+$: 463.10; Experimental: 463.09.

1-(4-((1-(2-(4-(benzothiazol-2-yl)phenoxy)ethyl)−1H-1,2,3-triazol-4-yl)methoxy)phenyl) ethan-1-one (**4d**): Off White solid, Yield: 87%, m.p. 138–140 °C. FT-IR (KBr, ν_{max}/cm^{-1}) = 3142, 2927, 2875, 1674, 1602, 1508, 1479, 1247, 1178 cm^{-1}. ^{1}H NMR (500 MHz, DMSO–d_6): δ = 2.54 (s, 3H, CH_3), 4.54 (t, J = 5.05 Hz, 2H, CH_2), 4.86 (t, J = 4.97 Hz, 2H, CH_2), 5.28 (s, 2H, CH_2), 7.11 (m, 2H),7.16 (m, 2H), 7.44 (m, 1H, Ar-H), 7.53 (ddd, 1H, J = 8.30, 7.18, 1.31 Hz Ar-H), 7.94 (m, 2H), 8.02 (m, 3H, Ar-H), 8.12 (d, J = 7.72 Hz, 1H), 8.41 (s, 1H, triazole-CH); ^{13}C NMR (125 MHz, DMSO–d_6): δ = 26.34, 48.95, 61.21, 66.38, 114.49, 115.30, 122.15, 122.44, 125.10, 125.36, 125.96, 126.47, 128.79, 130.04, 130.37, 134.19, 142.15, 153.57, 160.23, 161.75, 166.80, 196.22. ESI-MS (*m/z*) $C_{26}H_{23}N_4O_3S$: Calculated $[M + H]^+$: 471.15; Experimental: 471.15.

2-(4-(2-(4-((4-nitrophenoxy)methyl)−1H-1,2,3-triazol-1-yl) ethoxy)phenyl)benzothiazole (**4e**): Light brown solid, Yield: 83%, m.p. 122–124 °C. FT-IR (KBr, ν_{max}/cm^{-1}) = 3078, 2958, 2926, 1606, 1593, 1498, 1255, 1176, 1112 cm^{-1}. ^{1}H NMR (500 MHz, DMSO–d_6): δ = 4.54 (t, 2H, CH2), 4.87 (t, 2H, CH_2), 5.36 (s, 2H, CH_2), 7.03 (d, J = 8.88 Hz,1H), 7.11 (d, J = 8.35 Hz, 2H), 7.28 (d, J = 8.94 Hz, 1H, Ar-H), 7.44 (t, J = 7.30 Hz, 1H, Ar-H), 7.53 (m, J = 7.28 Hz 1H, Ar-H), 8.02 (d, J = 6.93 Hz, 4H), 8.12 (d, J = 8.18 Hz, 1H), 8.21 (d, J = 8.95 Hz, 1H, Ar-H, 8.45 (s, 1H, triazole-CH); ^{13}C NMR (125 MHz, DMSO–d_6): δ = 48.97, 61.78, 66.36, 115.26, 115.78, 122.12, 122.41, 125.07, 125.56, 125.73, 125.94, 125.98, 126.44, 128.76, 134.17, 140.91, 141.65, 153.54, 160.19, 163.16, 166.77. ESI- MS (*m/z*) $C_{24}H_{20}N_5O_4S$: Calculated $[M + H]^+$: 474.12; Experimental: 474.12.

2-(4-(3-(4-(phenoxymethyl)−1H-1,2,3-triazol-1-yl)propoxy) phenyl)benzothiazole (**4f**): Light brown solid, Yield: 91%, m.p. 108–110 °C. FT-IR (KBr, ν_{max}/cm^{-1}) = 3064, 3032, 2927, 2870, 1598, 1485, 1268, 1238, 1226, 1170 cm^{-1}. ^{1}H NMR (500 MHz, $CDCl_3$): δ = 2.33 (p, 2H, CH_2, J = 6.50 Hz), 4.08 (t, J = 6.00 Hz, 2H, CH_2), 4.59 (t, J = 6.92 Hz, 2H, CH_2), 5.14 (s, 2H, CH_2), 6.95 (d, J = 7.33 Hz,1H), 7.06 (m, 4H, Ar-H) 7.29 (dd, J = 8.69,7.36 Hz, 2H, Ar-H), 7.42 (m, 1H, Ar-H), 7.52 (m, 1H, Ar-H), 8.01 (dd, J = 8.78, 2.79 Hz, 2H, Ar-H), 8.10 (d, 1H, Ar-H, J = 8.00 Hz), 8.31 (s, 1H, triazole-CH); ^{13}C NMR (125 MHz, $CDCl_3$): δ = 29.26, 46.50, 60.92, 64.84, 114.56, 115.11, 120.71, 122.10, 122.38, 124.57, 125.01, 125.57, 125.01, 125.57, 126.42, 128.76, 129.40, 134.15, 142.68, 153.58, 157.95, 160.75, 166.91. ESI-MS (*m/z*) $C_{25}H_{23}N_4O_2S$: Calculated: $[M + H]^+$:443.15; Experimental: 443.15.

2-(4-(3-(4-((p-tolyloxy)methyl)−1H-1,2,3-triazol-1-yl)propoxy) phenyl)benzothiazole (**4g**): Off White solid, Yield: 93%, m.p. 134–136 °C. FT-IR (KBr, ν_{max}/cm^{-1}) = 3089, 3032, 2958, 2922, 1606, 1512, 1483, 1242, 1176 cm^{-1}. ^{1}H NMR (500 MHz, $CDCl_3$): δ = 2.22 (s, 3H, CH_3), 2.33 (m, 2H, CH_2), 4.08 (t, J = 6.01 Hz, 2H, CH_2), 4.57 (t, J = 6.92 Hz, 2H, CH_2), 5.09(s, 2H, CH_2), 6.91 (m, 2H), 7.08 (m, 4H), 7.42 (td, J = 7.71, 7.29, 1.15 Hz, 1H, Ar-H), 7.52 (m, 1H, Ar-H), 8.01 (m, 3H, Ar-H), 8.11 (dd, J = 7.97, 1.09 Hz, 1H,) 8.27 (s, 1H, triazole-CH); ^{13}C NMR (125 MHz, $CDCl_3$): δ = 19.97, 29.24, 46.49, 61.01, 64.84, 114.43, 115.12, 122.11, 122.38, 124.47, 125.02, 125.57, 126.43, 128.76, 129.36, 129.71, 134.14, 142.81, 153.57, 155.83, 160.75, 166.90. ESI-MS (*m/z*) $C_{26}H_{24}N_4O_2S$: Calculated $[M + H]^+$: 457.17; Experimental: 457.16.

2-(4-(3-(4-((4-chlorophenoxy)methyl)−1H-1,2,3-triazol-1-yl) propoxy)phenyl)benzothiazole (**4h**): Light brown solid, Yield: 83%, m.p. 120–122 °C. FT-IR (KBr, ν_{max}/cm^{-1}) = 3057, 2960, 2922, 2873, 1604, 1489, 1433, 1236, 1172 cm^{-1}. ^{1}H NMR (500 MHz, $CDCl_3$): δ = 2.34 (p, 2H, CH_2, J = 6.68 Hz), 4.09 (t, J = 5.97 Hz, 2H, CH_2), 4.59 (t, J = 6.90 Hz, 2H, CH_2), 5.16 (s, 2H, CH_2), 6.78 (m, 1H), 7.08 (dd, J = 8.95, 4.33 Hz 4H, Ar-H), 7.20 (m, 1H, Ar-H), 7.33 (m, 1H, Ar-H), 7.43 (m, 1H, Ar-H), 7.53 (m, 1H, Ar-H), 8.03 (m, 2H) 8.11 (d, 1H, Ar-H, J = 7.98 Hz) 8.30 (s, 1H, triazole-CH); ^{13}C NMR (125 MHz, $CDCl_3$): δ = 29.24, 46.52, 61.32, 64.82, 115.09, 116.40, 116.82, 122.09, 122.38, 124.46, 124.67, 124.81, 125.01, 125.58, 126.41, 128.76, 129.01, 129.13, 134.15, 142.33, 153.57, 156.22, 156.77, 160.74, 166.89. ESI-MS (*m/z*) $C_{25}H_{22}ClN_4O_2S$: Calculated $[M + H]^+$: 477.12; Experimental: 477.11

1-(4-((1-(3-(4-(benzothiazol-2-yl)phenoxy)propyl)−1H-1,2,3-triazol-4yl)methoxy)phenyl)ethan-1-one (**4i**): Light brown solid, Yield: 85%, m.p. 136–138 °C. FT-IR (KBr, ν_{max}/cm^{-1}) = 3055, 2958, 2918, 2850, 1670, 1600, 1483, 1361, 1247, 1180 cm^{-1}. ^{1}H NMR (500 MHz, $CDCl_3$): δ = 2.35 (m, 2H, CH_2), 2.52 (s, 3H, CH_3), 4.10 (t, 2H, CH_2), 4.61 (t, J = 6.30 Hz, 2H, CH_2), 5.27 (s, 2H, CH_2), 7.08 (d, 2H J = 8.27 Hz), 7.16 (d, 2H, J = 8.28 Hz), 7.44 (t, 1H, Ar-H), 7.53 (t, 1H, Ar-H), 7.94 (d, J = 8,29 Hz, 2H, Ar-H), 8.02 (d, 3H, Ar-H, J = 8.09 Hz), 8.12 (d, J = 7.74 Hz, 1H, Ar-H), 8.37 (s, 1H, triazole-CH); ^{13}C NMR (125 MHz, $CDCl_3$): δ = 26.31, 29.24, 46.56, 61.28, 64.86, 114.45, 115.11, 122.37, 124.85, 125.02, 125.56, 126.42, 128.76, 130.01, 130.35, 130.52, 134.14, 142.09, 153.57, 160.74, 161.75, 166.90, 196.20. ESI- MS (*m/z*) $C_{27}H_{25}N_4O_3S$: Calculated $[M + H]^+$: 485.16; Experimental: 485.16.

2-(4-(3-(4-((4-nitrophenoxy)methyl)−1H-1,2,3-triazol-1-yl) propoxy)phenyl)benzothiazole (**4j**): Light brown solid, Yield: 84%, m.p. 140–142 °C. FT-IR (KBr, ν_{max}/cm^{-1}) = 3080, 2926, 2873, 1606, 1496, 1435, 1342, 1257, 1172, 1112 cm^{-1}. ^{1}H NMR (500 MHz, DMSO- d_6): δ = 2.35 (m, J = 6.40 Hz, 2H, CH_2), 4.10 (t, J = 5.94 Hz, 2H, CH_2), 4.61 (t, J = 6.90 Hz, 2H, CH_2), 5.34 (s, 2H, CH_2), 7.08 (d, J = 8.83 Hz, 2H), 7.27 (d, 2H, J = 9.27 Hz, Ar-H), 7.43 (m, 1H, Ar-H), 7.52 (m, 1H, Ar-H), 8.02 (d, J = 8.73 Hz, 3H, Ar-H), 8.11 (d, J = 7.87 Hz 1H, Ar-H), 8.22 (d, J = 9.25 Hz, 2H, Ar-H), 8.36 (s, 1H, triazole-CH); ^{13}CNMR (125 MHz, DMS0-d_6): δ = 29.24, 46.61, 61.87, 64.85,115.09,115.22, 122.09, 122.39, 125.02, 125.59, 125.75, 126.42, 128.76, 134.16, 140.93, 141.69, 153.58, 160.73, 163.18, 166.89. ESI-MS (*m/z*) $C_{25}H_{22}N_5O_4S$: Calculated $[M + H]^+$: 488.14; Experimental: 488.13.

2-(4-(4-(4-(phenoxymethyl)−1H-1,2,3-triazol-1-yl)butoxy) phenyl)benzothiazole (**4k**): Off White solid, Yield: 92%, m.p. 120–122 °C. FT-IR (KBr, ν_{max}/cm^{-1}) = 3095, 2954, 2902, 2866, 1606, 1589, 1481, 1257, 1242, 1172 cm^{-1}. ^{1}HNMR (500 MHz, DMSO–d_6): δ = 1.73 (m, 2H, CH_2), 2.00 (m, 2H, CH_2), 4.09 (t, J = 6.32 Hz, 2H, CH_2), 4.47(t, J = 7.05 Hz, 2H, CH_2), 5.14 (s, 2H, CH_2), 6.95 (m, 1H, Ar-H), 7.04 (dd, J = 7.79 Hz and 1.01 Hz, 2H, Ar-H), 7.11 (m, 2H, Ar-H), 7.29 (m, 2H, Ar-H), 7.43 (td, 1H, J = 7.70 Hz and 7.29, 1.15 Hz, Ar-H), 7.52 (ddd, J = 8.29 Hz and 7.26 Hz, 1.25 Hz, 1H,Ar-H), 8.03 (m, 2H, Ar-H), 8.11 (m, 1H), 8.27 (s, 1H, triazole-CH). ^{13}CNMR (125 MHz, DMSO–d_6): δ = 25.50, 26.39, 49.00, 60.95, 67.05, 114.59, 115.13, 120.73, 122.11, 122.38, 124.36, 125.01, 125.41, 126.43, 128.78, 129.40, 134.15, 142.65, 153.60, 157.97, 160.98, 166.96. ESI- MS (*m/z*) $C_{26}H_{25}N_4O_2S$: Calculated $[M + H]^+$: 457.17; Experimental: 457.16.

2-(4-(4-(4-((p-tolyloxy)methyl)−1H-1,2,3-triazol-1-yl)butoxy) phenyl)benzothiazole (**4l**): Off-White solid, yield: 90%, m.p.138–140 °C. FT IR (KBr, ν_{max}/cm^{-1}) = 3089, 3032, 2951, 2868, 1606, 1516, 1483, 1247, 1174 cm^{-1}. ^{1}HNMR (500 MHz, $CDCl_3$): δ = 2.01 (m, 2H, CH_2), 2.27 (m, 5H), 4.19 (t, 2H, CH_2), 4.47 (t, 2H, CH_2), 5.16 (s, 2H, CH_2), 6.86 (d,2H), 6.98 (d,1H), 7.07 (d, 1H), 7.12 (t, 1H, Ar-H), 7.36 (t, 1H, Ar-H), 7.42 (t, 1H, Ar-H), 7.48 (t, 1H, Ar-H), 7.97 (d, 1H, Ar-H) 7.59 (s, 1H, triazole-CH), 8.08 (d, 1H, Ar-H) 8.52 (d, 1H, Ar-H); ^{13}C NMR (125 MHz, $CDCl_3$): δ = 20.0, 25.48, 26.38, 48.98, 61.04, 67.08, 114.46, 115.15, 122.13, 122.37, 124.36, 125.02, 125.40, 126.44, 128.78, 129.38, 129.73, 134.14, 142.72, 153.59, 155.85, 160.98, 166.98. ESI-MS $[M + H]^+$: *m/z* cal. for $C_{27}H_{28}N_4O_2S$ is 471.19, found 471.18.

2-(4-(4-(4-((4-chlorophenoxy)methyl)−1H-1,2,3-triazol-1-yl) butoxy)phenyl)benzothiazole (**4m**): Off-White solid, Yield: 86%, m.p. 128–130 °C. FT-IR (KBr, ν_{max}/cm^{-1}) = 3091, 2953, 2902, 2866, 1608, 1492, 1481, 1247, 1172 cm^{-1}. ^{1}H NMR (500 MHz, $CDCl_3$): δ = 1.73 (m, 2H, CH_2), 2.01 (m, 2H, CH_2), 4.09 (t, J = 6.46 Hz, 2H, CH_2), 4.47 (t, J = 7.04 Hz, 2H, CH_2), 5.14 (s, 2H, CH_2), 7.07 (m, 4H, Ar-H), 7.33 (m, 2H, Ar-H), 7.44 (dd, 1H, Ar-H), 7.52 (m, 1H, Ar-H), 8.02 (m, 3H, Ar-H), 8.11 (m, 1H, Ar-H), 8.27 (s, 1H, triazole-CH); ^{13}CNMR (125 MHz, $CDCl_3$): δ = 25.48, 26.37, 49.00, 61.35, 67.03, 115.12, 116.43, 122.10, 122.37, 124.46, 124.48, 125.01, 125.41, 126.43, 128.77, 129.14, 134.14, 142.29, 153.59, 156.79, 16 0.96, 166.95. ESI-MS (*m/z*) $C_{26}H_{24}ClN_4O_2S$: Calculated $[M + H]^+$: 491.13; Experimental: 491.12.

1-(4-((1-(4-(4-(benzothiazol-2-yl)phenoxy)butyl)−1H-1,2,3-triazol-4-yl)methoxy)phenyl) ethan-1-one (**4n**): Light brown solid, Yield: 85%, m.p. 138–140 °C. IR (KBr, ν_{max}/cm^{-1}) = 3095, 2960, 2872, 1680, 1597, 1483, 1471, 1255, 1176 cm^{-1}.^{1}HNMR (500 MHz, $CDCl_3$): δ = 1.73 (m, 2H, CH_2), 1.91 (s, 3H, CH_3) 2.02 (m, 2H, CH_2), 4.09 (t, J = 6.36 Hz, 2H, CH_2), 4.48 (t, J = 7.02 Hz, 2H, CH_2), 5.25 (s, 2H, CH_2), 7.11 (m, 2H), 7.15 (m, 2H, Ar-H), 7.43 (m, 1H, Ar-H), 7.52 (m, 1H, Ar-H), 7.93 (m, 2H, Ar-H), 8.03 (d, J = 8.86 Hz, 3H, Ar-H) 8.11 (d, J = 8.06 Hz, 1H, Ar-H) 8.31 (s, 1H, triazole-CH); ^{13}CNMR (125 MHz, $CDCl_3$): δ = 20.66, 25.48, 26.31, 49.03, 59.66, 67.03, 114.45, 115.13, 122.11, 122.37, 124.60, 125.02, 125.41, 126.43, 128.77, 130.03, 130.35, 134.14, 142.07, 153.5 9, 160.96, 161.76, 166.95, 170.25, 171.92, 196.20. ESI-MS (*m/z*) $C_{28}H_{27}N_4O_3S$: Calculated$[M + H]^+$: 499.18; Experimental: 499.17.

2-(4-(4-(4-((4-nitrophenoxy)methyl)−1H-1,2,3-triazol-1-yl) butoxy)phenyl)benzothiazoles (**4o**): Light brown solid, Yield: 80%, m.p. = 110–112 °C. FT-IR (KBr, ν_{max}/cm^{-1}) = 3078, 2945, 2927, 2868, 1608, 1595, 1512, 1496, 1257, 1111 cm^{-1}. ^{1}HNMR (500 MHz, $CDCl_3$): δ = 1.74 (m, 2H, CH_2), 2.03 (m, 2H, CH_2), 4.09 (t, J = 5.33 Hz, 2H, CH_2), 4.49 (t, J = 6.49 Hz, 2H, CH_2), 5.32 (s, 2H, CH_2), 6.94 (d, 1 H, Ar-H, J = 8.87 Hz), 7.10 (d, J = 8.27 Hz, 2H, Ar-H), 7.26 (d, J = 8.81 Hz, 2H, Ar-H), 7.42 (t, 1H, Ar-H, J = 7.27 Hz), 7.52 (t, J = 7.29 Hz, 1H, Ar-H), 8.02 (d, J = 8.18 Hz, 3H, Ar-H) 8.09 (d, J = 7.87 Hz, 1H, Ar-H), 8.21 (d, 1H, Ar-H, J = 8.74 Hz), 8.32 (s, 1H, triazole-CH); ^{13}CNMR (125 MHz, $CDCl_3$): δ = 25.48, 26.38, 49.07, 61.89, 67.02, 115.08, 115.20, 115.67, 122.05, 122.36, 124.76, 124.97, 125.43, 125.72, 126.05, 126.38, 128.75, 134.14, 140.94, 141.62, 153.59, 160.95, 163.19, 163.82, 166.92. ESI-MS (*m/z*) $C_{26}H_{24}N_5O_4S$: Calculated $[M + H]^+$: 502.15; Experimental: 502.14.

Credit author statement

Nidhi Nehra: Validation, Formal analysis, Investigation; **Ram Kumar Tittal:** Conceptualization, Methodology, Resources, Data Curation, Visualization, Writing -Original Draft, Writing- Review & Editing, Supervision; **Ghule Vikas D.:** Software, Data Curation; **Naveen:** Molinspiration Physicochemical Parameters Software **Kashmiri Lal:** Resources

Declaration of Competing Interest

The authors declare that they have no known competing financial interests or personal relationships that could have appeared to influence the work reported in this paper.

Acknowledgements

We acknowledge the Department of Chemistry, NIT Kurukshetra for the research facilities and financial assistance to NN as Institute Fellowship. Authors acknowledge Pardeep Kumar from Department of Microbiology, Kurukshetra University for Antifungal Studies. We also acknowledge SAIF Punjab University Chandigarh for NMR analysis and IIT Ropar, HRMS lab for ESI-MS facilities.

Supplementary materials

Supplementary material associated with this article can be found, in the online version, at doi:10.1016/j.molstruc.2021.131013.

References

[1] I. Manisalidis, E. Stavropoulou, A. Stavropoulos, E. Bezirtzoglou, Environmental and health impacts of air pollution: a review, Public Health Front. 8 (2020) 14.
[2] P.T.J. Johnson, S.H. Paull, The ecology and emergence of diseases in fresh waters, Freshw. Biol. 56 (4) (2011) 638–657.
[3] P.J. Landrigan, R. Fuller, N.J.R. Acosta, O. Adeyi, R. Arnold, N. Basu, A.B. Baldé, R. Bertollini, S. Bose-O'Reilly, J.I. Boufford, P.N. Breysse, T. Chiles, C. Mahidol, A.M. Coll-Seck, M.L. Cropper, J. Fobil, V. Fuster, M. Greenstone, A. Haines, D. Hanrahan, D. Hunter, M. Khare, A. Krupnick, B. Lanphear, B. Lohani, K. Martin, K.V. Mathiasen, M.A. McTeer, C.J.L. Murray, J.D. Ndahimananjara, F. Perera, J. Potočnik, A.S. Preker, J. Ramesh, J. Rockström, C. Salinas, L.D. Samson, K. Sandilya, P.D. Sly, K.R. Smith, A. Steiner, R.B. Stewart, W.A. Suk, O.C.P. van Schayck, G.N. Yadama, K. Yumkella, M. Zhong, The Lancet Commission on pollution and health, Lancet 391 (10119) (2018) 462–512.
[4] G. Janbon, J. Quintin, F. Lanternier, C. d'Enfert, Studying fungal pathogens of humans and fungal infections: fungal diversity and diversity of approaches, Genes Immun. 20 (5) (2019) 403–414.
[5] C. Firacative, Invasive fungal disease in humans: are we aware of the real impact? Mem. Inst. Oswaldo Cruz 115 (2020).
[6] R. Saral, Candida and Aspergillus Infections in Immunocompromised Patients: an Overview, Rev. Infect. Dis. 13 (3) (1991) 487–492.
[7] J. Houšť, J. Spížek, V. Havlíček, Antifungal Drugs, Metabolites 10 (3) (2020).
[8] M.J. Pucci, J.J. Bronson, J.F. Barrett, K.L. DenBleyker, L.F. Discotto, J.C. Fung-Tomc, Y. Ueda, Antimicrobial Evaluation of Nocathiacins, a Thiazole Peptide Class of Antibiotics, Antimicrob. Agents Ch. 48 (10) (2004) 3697.
[9] P.C. Sharma, K.K. Bansal, A. Sharma, D. Sharma, A. Deep, Thiazole-containing compounds as therapeutic targets for cancer therapy, Eur. J. Med. Chem. 188 (2020) 112016.
[10] J.M. Bueno, M. Carda, B. Crespo, A.C. Cuñat, C. de Cozar, M.L. León, J.A. Marco, N. Roda, J.F. Sanz-Cervera, Design, synthesis and antimalarial evaluation of novel thiazole derivatives, Bioorg. Med. Chem. Lett. 26 (16) (2016) 3938–3944.
[11] K.M. Dawood, T.M.A. Eldebss, H.S.A. El-Zahabi, M.H. Yousef, Synthesis and antiviral activity of some new bis-1,3-thiazole derivatives, Eur. J. Med. Chem. 102 (2015) 266–276.
[12] S. Cascioferro, B. Parrino, D. Carbone, D. Schillaci, E. Giovannetti, G. Cirrincione, P. Diana, Thiazoles, Their Benzofused Systems, and Thiazolidinone Derivatives: versatile and Promising Tools to Combat Antibiotic Resistance, J. Med. Chem. 63 (15) (2020) 7923–7956.
[13] K. Liaras, M. Fesatidou, A. Geronikaki, Thiazoles and Thiazolidinones as COX/LOX Inhibitors, Molecules 23 (3) (2018).
[14] A. Lauria, R. Delisi, F. Mingoia, A. Terenzi, A. Martorana, G. Barone, A.M. Almerico, 1,2,3-Triazole in Heterocyclic Compounds, Endowed with Biological Activity, through 1,3-Dipolar Cycloadditions, Eur. J. Org. Chem. 2014 (16) (2014) 3289–3306.
[15] Naveen, R. Kumar Tittal, G.D. Vikas, P. Rani, K. Lal, A. Kumar, Synthesis, Antimicrobial Activity, Molecular Docking and DFT Study: aryl-Carbamic Acid 1-Benzyl-1H-[1,2,3]Triazol-4-ylmethyl Esters, ChemistrySelect 5 (22) (2020) 6723–6729.
[16] S. Deswal, R.K.Tittal Naveen, D. Ghule Vikas, K. Lal, A. Kumar, 5-Fluoro-1H-indole-2,3-dione-triazoles- synthesis, biological activity, molecular docking, and DFT study, J. Mol. Struct. 1209 (2020) 127982.
[17] A. Rani, G. Singh, A. Singh, U. Maqbool, G. Kaur, J. Singh, CuAAC-ensembled 1,2,3-triazole-linked isosteres as pharmacophores in drug discovery: review, RSC Adv. 10 (10) (2020) 5610–5635.
[18] S. Deswal, R.K. Tittal, P. Yadav, K. Lal, G. VikasD, N. Kumar, Cellulose-Supported CuI-Nanoparticles-Mediated Green Synthesis of Trifluoromethylbenzoate-Linked Triazoles for Pharmacological & DFT study, ChemistrySelect 4 (2) (2019) 759–764.

[19] Naveen, R.K. Tittal, V.D. Ghule, N. Kumar, L. Kumar, K. Lal, A. Kumar, Design, synthesis, biological activity, molecular docking and computational studies on novel 1,4-disubstituted-1,2,3-Triazole-Thiosemicarbazone hybrid molecules, J. Mol. Struct. 1209 (2020) 127951.
[20] Naveen, R.K. Tittal, V.D. Ghule, P. Yadav, K. Lal, A. Kumar, Synthesis, antimicrobial potency with in silico study of Boc-leucine-1,2,3-triazoles, Steroids 161 (2020) 108675.
[21] Naveen, R.K. Tittal, P. Yadav, K. Lal, G.V. D, A. Kumar, Synthesis, molecular docking and DFT studies on biologically active 1,4-disubstituted-1,2,3-triazole-semicarbazone hybrid molecules, New J. Chem. 43 (21) (2019) 8052–8058.
[22] M. Gümüş, M. Yakan, İ. Koca, Recent advances of thiazole hybrids in biological applications, Future Med Chem 11 (15) (2019) 1979–1998.
[23] K. Bozorov, J. Zhao, H.A. Aisa, 1,2,3-Triazole-containing hybrids as leads in medicinal chemistry: a recent overview, Bioorg. Med. Chem. 27 (16) (2019) 3511–3531.
[24] R.M. Kumbhare, U.B. Kosurkar, M. Janaki Ramaiah, T.L. Dadmal, S.N.C.V.L. Pushpavalli, M. Pal-Bhadra, Synthesis and biological evaluation of novel triazoles and isoxazoles linked 2-phenyl benzothiazole as potential anticancer agents, Bioorg. Med. Chem. Lett. 22 (17) (2012) 5424–5427.
[25] S. Maračić, T.G. Kraljević, H.Č. Paljetak, M. Perić, M. Matijašić, D. Verbanac, M. Cetina, S. Raić-Malić, 1,2,3-Triazole pharmacophore-based benzofused nitrogen/sulfur heterocycles with potential anti-Moraxella catarrhalis activity, Bioorg. Med. Chem. 23 (23) (2015) 7448–7463.
[26] T.G. Kraljević, A. Harej, M. Sedić, S.K. Pavelić, V. Stepanić, D. Drenjančević, J. Talapko, S. Raić-Malić, Synthesis, in vitro anticancer and antibacterial activities and in silico studies of new 4-substituted 1,2,3-triazole–coumarin hybrids, Eur. J. Med. Chem. 124 (2016) 794–808.
[27] N. Rezki, A Green Ultrasound Synthesis, Characterization and Antibacterial Evaluation of 1,4-Disubstituted 1,2,3-Triazoles Tethering Bioactive Benzothiazole Nucleus, Molecules 21 (4) (2016) 505-505.
[28] C.G. Ricci, P.A. Netz, Docking Studies on DNA-Ligand Interactions: building and Application of a Protocol To Identify the Binding Mode, J. Chem. Inf. Model. 49 (8) (2009) 1925–1935.
[29] R. Santosh, M.K. Selvam, S.U. Kanekar, G.K. Nagaraja, M. Kumar, Design, Synthesis, DNA Binding, and Docking Studies of Thiazoles and Thiazole-Containing Triazoles as Antibacterials, ChemistrySelect 3 (14) (2018) 3892–3898.
[30] N.Ö. Can, U.Acar Çevik, B.N. Sağlık, S. Levent, B. Korkut, Y. Özkay, Z.A. Kaplancıklı, A.S. Koparal, Synthesis, Molecular Docking Studies, and Antifungal Activity Evaluation of New Benzimidazole-Triazoles as Potential Lanosterol 14α-Demethylase Inhibitors, J Chem 2017 (2017) 9387102.
[31] G.M. Morris, R. Huey, W. Lindstrom, M.F. Sanner, R.K. Belew, D.S. Goodsell, A.J. Olson, AutoDock4 and AutoDockTools4: automated docking with selective receptor flexibility, J. Comput. Chem. 30 (16) (2009) 2785–2791.
[32] C. Butnarasu, N. Barbero, G. Viscardi, S. Visentin, Unveiling the interaction between PDT active squaraines with ctDNA: a spectroscopic study, Spectrochim. Acta A 250 (2021) 119224.
[33] N. Nehra, R. Kumar Tittal, V.D. Ghule, N. Kumar, A. Kumar Paul, K. Lal, A. Kumar, CuAAC Mediated Synthesis of 2-HBT Linked Bioactive 1,2,3-Triazole Hybrids: investigations through Fluorescence, DNA Binding, Molecular Docking, ADME Predictions and DFT Study, ChemistrySelect 6 (4) (2021) 685–694.
[34] N. Nehra, R. Kaushik, G. Vikas D, R.K. Tittal, Simpler molecular structure as selective & sensitive ESIPT-based fluorescent probe for cysteine and Homocysteine detection with DFT studies, J. Mol. Struct. 1207 (2020) 127839.
[35] E. Buraka, C.Y.-C. Chen, M. Gavare, M. Grube, G. Makarenkova, V. Nikolajeva, I. Bisenieks, I. Brūvere, E. Bisenieks, G. Duburs, N. Sjakste, DNA-binding studies of AV-153, an antimutagenic and DNA repair-stimulating derivative of 1,4-dihydropiridine, Chem. Biol. Interact. 220 (2014) 200–207.
[36] S. Brogi, T.C. Ramalho, K. Kuca, J.L. Medina-Franco, M. Valko, Editorial: in silico Methods for Drug Design and Discovery, Front Chem 8 (2020) 612.
[37] B. Shah, P. Modi, S.R. Sagar, In silico studies on therapeutic agents for COVID-19: drug repurposing approach, Life Sci. 252 (2020) 117652.
[38] T. Kampmann, R. Yennamalli, P. Campbell, M.J. Stoermer, D.P. Fairlie, B. Kobe, P.R. Young, In silico screening of small molecule libraries using the dengue virus envelope E protein has identified compounds with antiviral activity against multiple flaviviruses, Antivir. Res. 84 (3) (2009) 234–241.
[39] F. Shaikh, Y. Zhao, L. Alvarez, M. Iliopoulou, C. Lohans, C.J. Schofield, S. Padilla–Parra, S.W.I. Siu, E.E. Fry, J. Ren, D.I. Stuart, Structure-Based in Silico Screening Identifies a Potent Ebolavirus Inhibitor from a Traditional Chinese Medicine Library, J. Med. Chem. 62 (6) (2019) 2928–2937.
[40] A. Daina, O. Michielin, V. Zoete, SwissADME: a free web tool to evaluate pharmacokinetics, drug-likeness and medicinal chemistry friendliness of small molecules, Sci. Rep. 7 (1) (2017) 42717.
[41] C.A. Lipinski, F. Lombardo, B.W. Dominy, P.J. Feeney, Experimental and computational approaches to estimate solubility and permeability in drug discovery and development settings1PII of original article: S0169-409X(96)00423-1. The article was originally published in Advanced Drug Delivery Reviews 23 (1997) 3–25.1, Adv. Drug Deliv. Rev. 46 (1) (2001) 3–26.
[42] I. Piyanzina, B. Minisini, D. Tayurskii, J.-.F. Bardeau, Density functional theory calculations on azobenzene derivatives: a comparative study of functional group effect, J. Mol. Model. 21 (2) (2015) 34.
[43] M.F. Khan, N. Nahar, R.B. Rashid, A. Chowdhury, M.A. Rashid, Computational investigations of physicochemical, pharmacokinetic, toxicological properties and molecular docking of betulinic acid, a constituent of Corypha taliera (Roxb.) with Phospholipase A2 (PLA2), BMC Complement. Altern. Med. 18 (1) (2018) 48.
[44] S.K. Lee, I.H. Lee, H.J. Kim, G.S. Chang, J.E. Chung, K.T. No, The PreADME Approach: web-based program for rapid prediction of physico-chemical, drug absorption and drug-like properties, EuroQSAR designing drugs and crop protectants: processes, problems and solutions (2003) 418–420.
[45] S.K. Lee, G.S. Chang, I.H. Lee, J.E. Chung, K.Y. Sung, K.T. No, The PreADME: pc-based program for batch prediction of adme properties, EuroQSAR 9 (2004) 5–10.
[46] G.W.T.M.J. Frisch, H.B. Schlegel, G.E. Scuseria, M.A. Robb, J. R., G.S. Cheeseman, V. Barone, G.A. Petersson, H. Nakatsuji, X. Li, A.V.M.M. Caricato, J. Bloino, B.G. Janesko, R. Gomperts, B., H.P.H. Mennucci, J.V. Ortiz, A.F. Izmaylov, J.L. Sonnenberg, F.D. Williams, F. Lipparini, F. Egidi, J. Goings, B. Peng, A. Petrone, T., D.R. Henderson, V.G. Zakrzewski, J. Gao, N. Rega, G. Zheng, M.H.W. Liang, M. Ehara, K. Toyota, R. Fukuda, J. Hasegawa, M., T.N. Ishida, Y. Honda, O. Kitao, H. Nakai, T. Vreven, K. Throssell, J.E.P.J.A. Montgomery Jr., F. Ogliaro, M.J. Bearpark, J.J. Heyd, K.N.K.E.N. Brothers, V.N. Staroverov, T.A. Keith, R. Kobayashi, J., K.R. Normand, A.P. Rendell, J.C. Burant, S.S. Iyengar, J., M.C. Tomasi, J.M. Millam, M. Klene, C. Adamo, R. Cammi, J. W., R.L.M. Ochterski, K. Morokuma, O. Farkas, J.B. Foresman, D.J. Fox, Gaussian 09 Rev. E.01, Wallingford, CT (2009).
[47] L.H. Mendoza-Huizar, C.H. Rios-Reyes, Chemical Reactivity of Atrazine Employing the Fukui Function, J. Mex. Chem. Soc. 55 (2011) 142–147.
[48] M. Elango, R. Parthasarathi, V. Subramanian, U. Sarkar, P.K. Chattaraj, Formaldehyde decomposition through profiles of global reactivity indices, J. Mol. Struct.: THEOCHEM 723 (1) (2005) 43–52.
[49] T. Koopmans, Über die Zuordnung von Wellenfunktionen und Eigenwerten zu den Einzelnen Elektronen Eines Atoms, Physica 1 (1) (1934) 104–113.
[50] R.G. Parr, L.v. Szentpály, S. Liu, Electrophilicity Index, J. Am. Chem. Soc. 121 (9) (1999) 1922–1924.
[51] C. Lee, W. Yang, R.G. Parr, Development of the Colle-Salvetti correlation-energy formula into a functional of the electron density, Phys. Rev. B 37 (2) (1988) 785–789.
[52] A.D. Becke, Density-functional thermochemistry. III. The role of exact exchange, J. Chem. Phys. 98 (7) (1993) 5648–5652.
[53] L.D. Sabath, The assay of antimicrobial compounds, Hum. Pathol. 7 (3) (1976) 287–295.
[54] A.A. Miles, S.S. Misra, J.O. Irwin, The estimation of the bactericidal power of the blood, Epidemiol. Infect. 38 (6) (1938) 732–749.
[55] N. Kuntala, J.R. Telu, V. Banothu, S.B. Nallapati, J.S. Anireddy, S. Pal, Novel benzoxepine-1,2,3-triazole hybrids: synthesis and pharmacological evaluation as potential antibacterial and anticancer agents, MedChemComm 6 (9) (2015) 1612–1619.
[56] A.K. Jordão, P.C. Sathler, V.F. Ferreira, V.R. Campos, M.C.B.V. de Souza, H.C. Castro, A. Lannes, A. Lourenco, C.R. Rodrigues, M.L. Bello, M.C.S. Lourenco, G.S.L. Carvalho, M.C.B. Almeida, A.C. Cunha, Synthesis, antitubercular activity, and SAR study of N-substituted-phenylamino-5-methyl-1H-1,2,3-triazole-4-carbohydrazides, Bioorg. Med. Chem. 19 (18) (2011) 5605–5611.